COMBINED SATELLITE OBSERVATION AND MODELING THE WAVES IN TROPICAL CYCLONES

Maria Yurovskaya[1,2], Alexis Mouche[3], Alexey Mironov[4], Fabrice Collard[5], Betrand Chapron[3], Vladimir Kudryavtsev[2,1]

[1]Marine Hydrophysical Institute, Sevastopol, Russia,
Email: mvkosnik@gmail.com
[2]Russian State Hydrometeorological University, St. Petersburg,
Email: kudr@rhmu.ru
[3]IFREMER, Brest, France,
Email: Alexis.Mouche@ifremer.fr
[4]eOdyn, Brest, France,
Email: wavedissipation@gmail.com,
[5]OceanDataLab, Brest, France,
Email: dr.fab@oceandatalab.com

KEY WORDS: tropical cyclone, wave modeling, CFOSAT SWIM, SAR, hazard prediction

ABSTRACT: A joint analysis of CFOSAT SWIM/SCAT and Sentinel-1 SAR data together with results of recently developed parametric model for rapid estimation of waves in tropical cyclones (TC) is presented. The satellite measurements were obtained over the Philippine Sea on October 29th, 2020, in TC Goni. The model for wave evolution inside TC is based on energy and momentum conservation laws. The coupled equations are written in their characteristic form to provide practical means to rapidly assess how the energy, frequency and direction of dominant surface waves are developing under varying wind forcing conditions and how the waves leave the storm area as swell systems. Being tested on a number of cyclones with different parameters (maximum wind speed u_m, TC radius R_m and heading velocity V), the model results have been reduced to analytical self-similar solution (TC-wave geophysical model function (GMF)) for the immediate first-guess estimate of significant wave height, wavelength and wave direction fields generated by an arbitrary cyclone characterized by a set of u_m, R_m and V.

Results of wave modeling with the wind field input either from Sentinel-1 SAR or CFOSAT SCAT data are compared to CFOSAT SWIM measurements, including altimeter ones. The wave fields inside moving cyclones usually exhibit a strong azimuthal asymmetry, resulting from a resonance between wave group velocity and TC heading velocity. For TC Goni, this effect is well captured, leading to extreme waves with heights up to 8 m, further outrunning as swell with wavelength about 250 m in the TC heading direction. A quantitative agreement between the satellite measurements and model results (both the direct model and its simplified solutions) is observed. In the far zone (~10 R_m) local wind is found to be the leading factor of wave formation.

The case study demonstrates that combined radar, altimeter, scatterometer data, numerical modeling and analytical self-similar solutions open new perspectives to study the waves generated by TCs for different scientific and practical purposes including hazard prediction.

1. INTRODUCTION

Observation and modeling the waves in tropical cyclones (TC) is of great scientific and practical interest due to their important role in air-ocean coupled system and potential hazard to shipping and coastal infrastructure. Remote and *in situ* ocean observations and numerical predictions assimilating this data have been greatly improved in last decades. Besides a number of altimeters, scatterometers, radar and optical instruments, new missions combining different sensors are being developed and launched. For example, the instrument onboard Sentinel-3 satellite developed by the European Space Agency includes surface temperature radiometer, optical scanners, synthetic aperture radar altimeter and microwave radiometer to measure topography, temperature, ocean pollution and many other characteristics for marine forecasting and monitoring (Donlon et al., 2012). The satellite mission CFOSAT (China France Oceanography Satellite), started in 2018, is the first one aimed to obtain simultaneously both the ocean surface wind and wave two-dimensional information. The instruments onboard CFOSAT are SCAT, a wind-field scatterometer, and a unique real-aperture scanning radar system SWIM (Surface Waves Investigation and Monitoring), producing the directional spectra of ocean waves. The main CFOSAT objective is to systematically monitor wind and waves on a global scale and to provide information on related ocean and atmospheric applications (Hauser et al., 2019).

Despite a thorough continuous space-borne and in-field (buoys) monitoring of ocean state, extreme weather

events still lack precise information on wind fields, waves and outrunning swell. Thus, the wave modeling remains the principal instrument for proper forecasting of waves generated by TCs. The study performed by Moon et al. (2003), combining WAVEWATCH III numerical model and scanning radar altimeter measurements inside TC Bonnie, demonstrates the model capability to reproduce the wave fields in extreme wind conditions. A simpler and less time/power consuming way for wave modeling in TC conditions was presented recently by Kudryavtsev et al. (2021a,b). The authors suggest a physically grounded and easy-to-use two-dimensional parametric model for describing the statistical characteristics of surface waves. From a series of numerical experiments, the simplified self-similar solutions were obtained for the first-guess estimate of waves in arbitrary TC defined by its radius, translation velocity and maximum wind speed. The model was tested on different in-field and satellite measurements and good agreement of predicted and observed wave fields was demonstrated. Particularly, it reproduces the well-know effect of waves intensification in the forward/right TC sector (relatively to the heading) resulting from a resonance between wave group velocity and TC heading velocity.

The aim of this work is to reveal the capabilities and advantages of combining a new numerical model, CFOSAT SWIM measurements, radar and altimeter data for investigating and predicting the waves generated by TCs. The study was motivated by a case of hurricane Goni (2020) in the Phillipine Sea, quasi-synchronously overlapped by large-swath CFOSAT data and high-resolution Sentinel-1 SAR measurements to provide precise wind information for wave modeling. The model and satellite data description, their application and comparison are presented below.

2. MODELING THE WAVES IN TC

2.1 Governing Equations

The two-dimensional parametric model is based on energy and momentum conservation laws (Hasselmann et al., 1976) with the use of self-similar fetch laws for wind waves development (Kitaigorodskii, 1962). Equations deduction and detailed description of model parameters are given in Kudryavtsev (2021a). The final system of equations for wave evolution and swell propagation in the wind field varying in space and time reads:

$$\frac{d}{dt}\ln(\overline{c}_g e) = -\overline{c}_g G_n + \omega_p \left(\tilde{I}_w - \tilde{D} \right)$$

$$\frac{d}{dt}c_{gp} = -\frac{r_g C_\alpha}{2}\Delta_p g \left(k_p^2 e \right)^2$$

$$\frac{d}{dt}\varphi_p = -C_\varphi \left(\frac{u_{10}}{c_p} \right)^2 \omega_p H_p \sin\left[2(\varphi_p - \varphi_W) \right]$$

$$\frac{dx}{dt} = \cos(\varphi_p)\overline{c}_g \qquad \frac{dy}{dt} = \sin(\varphi_p)\overline{c}_g ,$$

(1)

where e is the total wave energy, $\overline{c}_g$ is the mean group velocity weighted over spectrum; ω_p, c_{gp}, c_p and k_p are frequency, group velocity, phase velocity and wavenumber of spectral peak, respectively; u_{10} is wind speed at 10 meters above the sea level; φ_w and φ_p are wind and wave spectral peak directions; g is gravity; x and y are wave train coordinates, $\tilde{I}_w$ is the dimensionless energy wind input and $\tilde{D}$ is the dimensionless energy dissipation due to wave breaking; term G_n describes the effects of wave field convergence/divergence and $r_g, C_a, C_\varphi, \Delta_p, H_p$ are dimensionless constants and functions described in Kudryavtsev (2021a), Appendix 2.

System (1) is solved iteratively using the ray-tracing method in moving TC reference system. A ray superposition visualizes how the energy, frequency and direction of dominant surface waves evolve and how the waves leave the storm area as swell systems.

2.2 TC-wave GMF

As well as in the case of wave development in uniform wind conditions, wave characteristics in TC are anticipated to obey self-similar laws (Kudryavtsev et al., 2015; Young, 2017). In order to establish these laws, the parametric model was run for a set of wind field parameters (TC radius R_m, maximum wind speed u_m) and different TC heading velocities V. The results were generalized into self-similar analytical solutions as follows (Kudryavtsev et al., 2021).

Maximal waves generated by a moving TC are approximated as:

$$(e^{max}/e_0^{max})_{slow} = 1 + 3.84 \cdot (R_m/L_{cr})^{-0.4}$$
$$(\lambda^{max}/\lambda_0^{max})_{slow} = 1 + 1.37 \cdot (R_m/L_{cr})^{-0.38}$$
$$(e^{max}/e_0^{max})_{fast} = 2.92 \cdot (R_m/L_{cr})^{0.53}$$
$$(\lambda^{max}/\lambda_0^{max})_{fast} = 1.67 \cdot (R_m/L_{cr})^{0.31}$$

(2)

where $Lcr = 6.46e3 \cdot (u_m^2/g)(u_m/2V)^{-4}$ is the critical fetch meaning the distance from the initial point of wave train generation to the turning point where the wave group velocity becomes equal to the TC translation velocity. Index "slow"/"fast" separates the two regimes: $R_m/L_{cr} > 1$ (''slow'' TC), and $R_m/L_{cr} < 1$ (''fast'' TC). In the latter case the TC heading velocity is too large, and all waves "slide down" to the backward TC sector. The region around $R_m/L_{cr} = 1$ corresponds to the group velocity resonance conditions, leading to the largest possible waves generated by a TC; $e_0^{max}, \lambda_0^{max}$ are the energy and wavelength of maximum waves generated by a TC with the same parameters but zero translation velocity:

$$e_0^{max} = 1.4 \cdot 10^{-6} (u_m^4/g^2)(R_m g/u_m^2)^{3/4}$$
$$\lambda_0^{max} = 6 \cdot 10^{-2} (u_m^2/g)(R_m g/u_m^2)^{1/2}$$

(3)

In two-dimensional case the wave energy, wavelength and wave direction of primary wave trains are also normalized by their corresponding stationary values (analytical expressions are given e.g. in Kudryavtsev et al., 2021b) and represented as functions of TC azimuth and $r = L_{cr}'$ (r the distance from TC center and L_{cr}' is defined for the local wind speed). These two-dimensional matrices can be viewed as TC-wave Geophysical Model Function (TC-wave GMF) to analytically derive 2D field of significant wave height (Hs), wavelength and direction fields. A clear advantage of these 2D self-similar solutions is a rapid and efficient quantitative first-guess estimate of waves generated by an arbitrary TC prescribed by R_m, u_m and V.

2.2 Swell

In the far zone, outside wave generation area, the swell rays can be parameterized by expressions following from the first two equations in (1):

$$(e_0/e)^2 = (\chi^2 + \delta^2)\left[\frac{1}{1+\delta^2} + \frac{A}{\delta}\left(\tan^{-1}\frac{\chi}{\delta} - \tan^{-1}\frac{1}{\delta}\right)\right]$$
$$(\lambda/\lambda_0)^5 - 1 = \frac{b}{4}\ln\left[1 + A\frac{1+\delta^2}{\delta}\left(\tan^{-1}\frac{\chi}{\delta} - \tan^{-1}\frac{1}{\delta}\right)\right]$$

(4)

where $\chi = 1 + G_0 x$, $\delta = 0.1$, $A = 4(k_{p0}/G_0)(k_{p0}e_0/\varepsilon_T^2)^2$, $b = 0.59$, $\varepsilon_T = 0.155$; $G_0 = d\varphi_p/dn$ is the gradient of wave peak direction across the wave propagation direction; x is the length of swell ray and zeros indicate here the wave train parameters at $x=0$. Approximation (4) accounts both the swell dissipation and focusing/defocusing effects.

3. A CASE STUDY AND SATELLITE DATA

To apply the parametric model, the wind field and TC speed are needed as input. Generally, the wind field is asymmetric and can vary in time, but for simplicity, in practice it can be considered stable and described by a Holland (1980) function using only R_m, u_m and parameter B:

$$u(r) = \left[\left(u_m^2 + u_m rf\right)\left(\frac{R_m}{r}\right)^B \exp\left(-\left(\frac{R_m}{r}\right)^B + 1\right) + \left(\frac{rf}{2}\right)^2\right]^{1/2} - \frac{rf}{2} \cdot$$

(5)

TC trajectory is then can be taken as a straight line with constant heading velocity during 1-2 days. While these assumptions are optional in direct model calculation, they are necessary for TC-wave GMF.

One of the cases when these conditions were close to reality is TC Goni, the second most intense cyclone in 2020.

It intensified over the Philippine Sea on October 29th and became a category 5 super typhoon on October 30th, with maximum winds speeds up to 85 m/s. TC track is shown on Fig. 1a, where color indicates the maximum wind speed. Parameters u_m, R_m and V along track (the Best Track Data), are given on Fig. 1b.

The data for this research was mostly provided by CyclObs (cyclobs.ifremer.fr/app), a project led by IFREMER to build a unique database of satellite and in situ data on TCs. The wind field information was obtained from CFOSAT SCAT (scatterometer) and Sentinel-1A (SAR) instruments. On October 29th, tracks of the two satellites passed very close to Goni eye almost at the same time (22:11 and 20:57, respectively). These two types of measurements complement each other well: while SAR data is fine-resolved on a swath of hundreds km, CFOSAT SCAT provides ~1000 km width observations with 25 km resolution (Fig. 1c).

Wave measurements are performed by CFOSAT SWIM instrument, which is a Ku-band radar with a near-nadir scanning beam geometry designed to measure the spectral properties of surface ocean waves (Hauser et al., 2021). Directional wave spectra and their parameters are recovered from off-nadir measurements conducted by rotating beams pointing at 6°, 8°, 10° mean incidences (a spiral-like line on Fig.1c). SWIM nadir products include significant wave height (Hs) and wind speed with accuracy similar to standard altimeter missions (Liang et al., 2021). The region of the cyclone in its intensive phase was crossed by CFOSAT tracks thrice (1S, 2S, 3S on Fig. 1), but we focus on October 29th case (1S), the only one when the TC center was covered by SWIM measurements. We consider also Jason-1 altimeter data, whose track passed through the backward (relative to the heading) TC zone. All altimeters tracks in coordinate system related to the cyclone center are shown on Fig.3e.
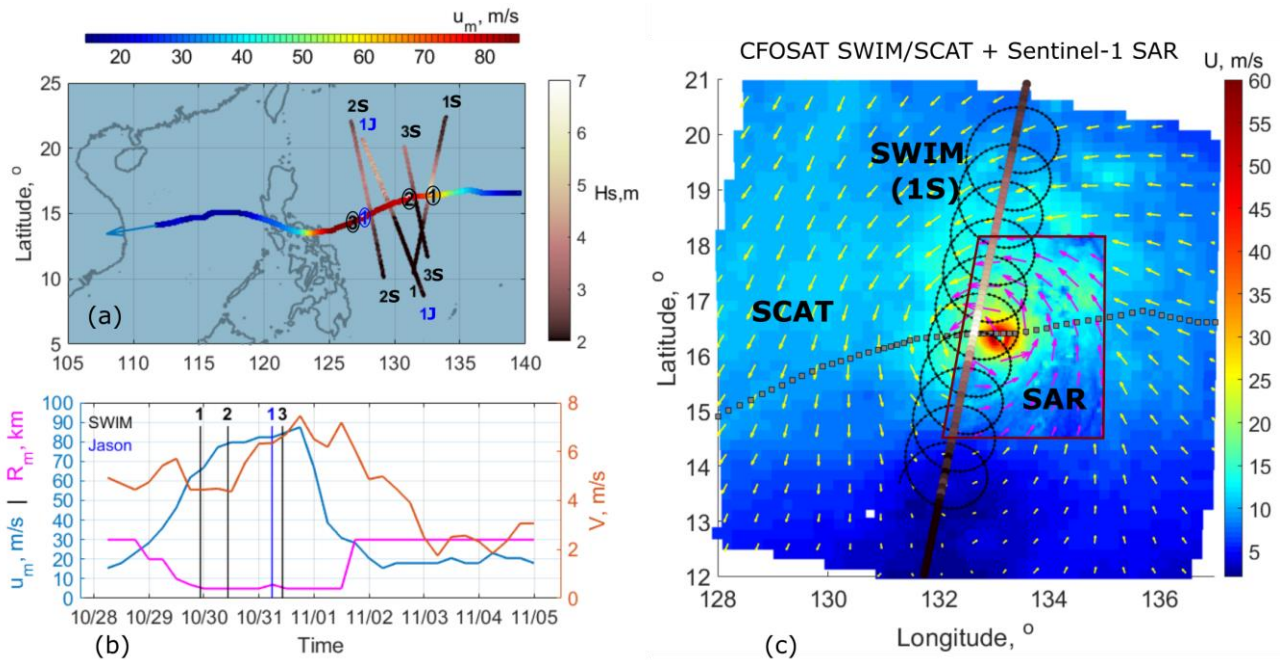

Figure 1. (a) TC Goni track and Hs altimeter measurements. Circled numbers indicate TC location at time of satellite passage. (b) Time evolution of Goni parameters. (c) Wind fields from CFOSAT SCAT and Sentinel-1A SAR data (outlined polygon), TC track (gray squares), CFOSAT SWIM nadir Hs (the same colormap as on subplot (a)) and SWIM rotating beam track with 10° incidence angle (black dots).

As the TC radius is of order of 10 km, CFOSAT SCAT 25 km-resolution measurements cannot provide accurate wind information in TC wave-generation zone. Moreover, scatterometer wind-retrieval algorithm fails at winds higher than 20 m/s and in rain presence. An accurate estimate of the ocean surface wind speed and direction was obtained from Sentinel-1 measurements using the new algorithm suggested for SAR data (Duong et al., 2021). The inversion scheme is based on high sensitivity of C-band VH measurements to the wind speed, including the measurements in extreme events (Mouche et al., 2017, 2019). After TC center detection, it is used to constrain a parametric inflow model (Zhang and Uhlhorn, 2012) in the storm frame of reference for a full estimate of the wind direction with the same resolution as the wind speed. The method gives the wind field with resolution ~1 km (Fig. 2a). Comparison of wind speed radial distributions from SCAT and SAR data (Fig. 2b) shows their accordance outside the distance ~70 km from TC center. At smaller distances SCAT-derived wind speed is underestimated and only the wind from SAR is applicable. For direct 2D parametric model the wind field presented on Fig. 2a will be used, and for TC-wave GMF it will be approximated with an azimuthally symmetric function (5) with parameters $R_m = 15$ km, $u_m = 47$ m/s, $B = 1.9$ (the black line on Fig. 2b).

Far from TC center, the wind waves energy will be estimated using CFOSAT SCAT data considering the waves

to be fully developed and obey Pierson-Moskowitz (1964) law:

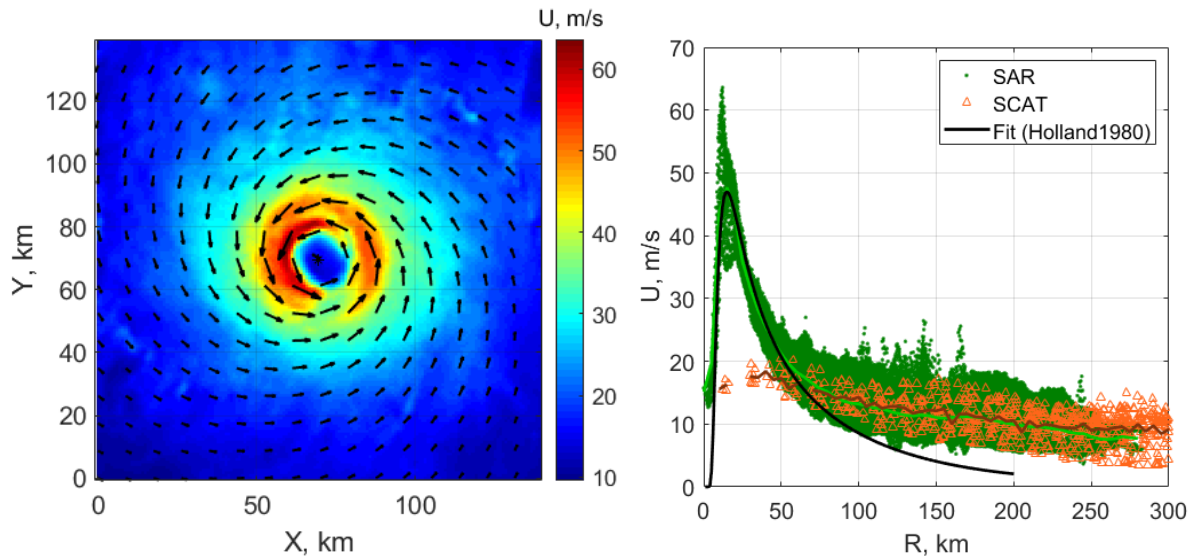$$e = 2.7 \cdot 10^{-3} \cdot u_{10}^{4} / g^{2} . \tag{6}$$

Figure 2. (a) Wind field inside TC Goni retrieved from Sentinel-1 SAR. (b) Wind speed profiles from SAR (green) and CFOSAT SCAT (orange) data. Solid lines are respective 5 km-binned average; black solid line is Holland (1980) approximation of SAR-derived wind field.

4. RESULTS

4.1 Significant Wave Height and Wavelength

As a first step, the maximum waves generated by the TC were estimated using Eq. (1)-(2). The parameters $R_m = 15$ km, $u_m = 47$ m/s and $V=5.5$ m/s give $R_m/L_{cr} = 2.9$ ("slow" TC), maximum wave height 9.4 m and wavelength 205 m. SWIM nadir Hs (track 1S) has the maximum value about 8 m, while spectrum from off-nadir measurements has the peak at about 200 m wavelength. Notice that at the distance of more than 2-3 TC radii the longest waves turn to swell regime. They lose their energy due to wave breaking dissipation but keep the wavelength almost constant. Thus the estimates of Eq. (1)-(2) are adequate.

The fields of significant wave height and wavelength calculated using 2D parametric model with wind input shown on Fig. 2a and TC translation velocity 5.5 m/s are presented on Fig. 3a-b. As anticipated, the strongest waves are observed in the right-front TC sector (relative to the heading) due to the wave group velocity resonance. These waves then turn left following the wind direction and leave TC through the front and front-right sector as 200 m swell.

Similar result is obtained using TC-wave GMF, Fig. 3c-f. A gray contour on Fig. 3c-d corresponds to the transition to swell regime where GMF is inapplicable. The wave field outside the wave generation area is the interpolation of wave characteristics of swell rays (4) starting from the contour with initial wave height, wavelength and direction predicted by TC-wave GMF.

As obtained, Fig. 3a,c,e, the direct model and the TC-wave GMF with swell approximation well reproduce the observed Hs values along SWIM track 1S. Hs profiles are compared on Fig. 3g. Close to TC center both the model (blue) and GMF (black line) agree well with altimeter data (red). At $Y > 100$ km, GMF-derived Hs (the swell part) is underestimated presumably due to the presence of underlying wind waves which are not accounted by TC-wave GMF. In direct model prediction all the waves are considered, but calculations on a fine grid are rather time- and power-consuming and we limited them within the area 150 x 150 km (the one, where SAR data is available in all TC sectors). To fill this gap, CFOSAT SCAT data can be used to roughly assess the impact of shorter wind waves. Gray dashed line shows the upper estimate: height of the fully developed waves under the action of local wind, Eq. (6). In the left TC sector (relative to the heading, $Y<0$), far from the eye, wind waves are much smaller than swell generated by the TC, and GMF fully describes the waves in this region. In the right sector, where the wind is stronger (see Fig. 1c), the account of local wind sea is necessary. At distances larger than 200 km ($\sim10R_m$) the superposition of GMF- and SCAT-derived waves (the green line) gives Hs level, coinciding with altimeter measurements.
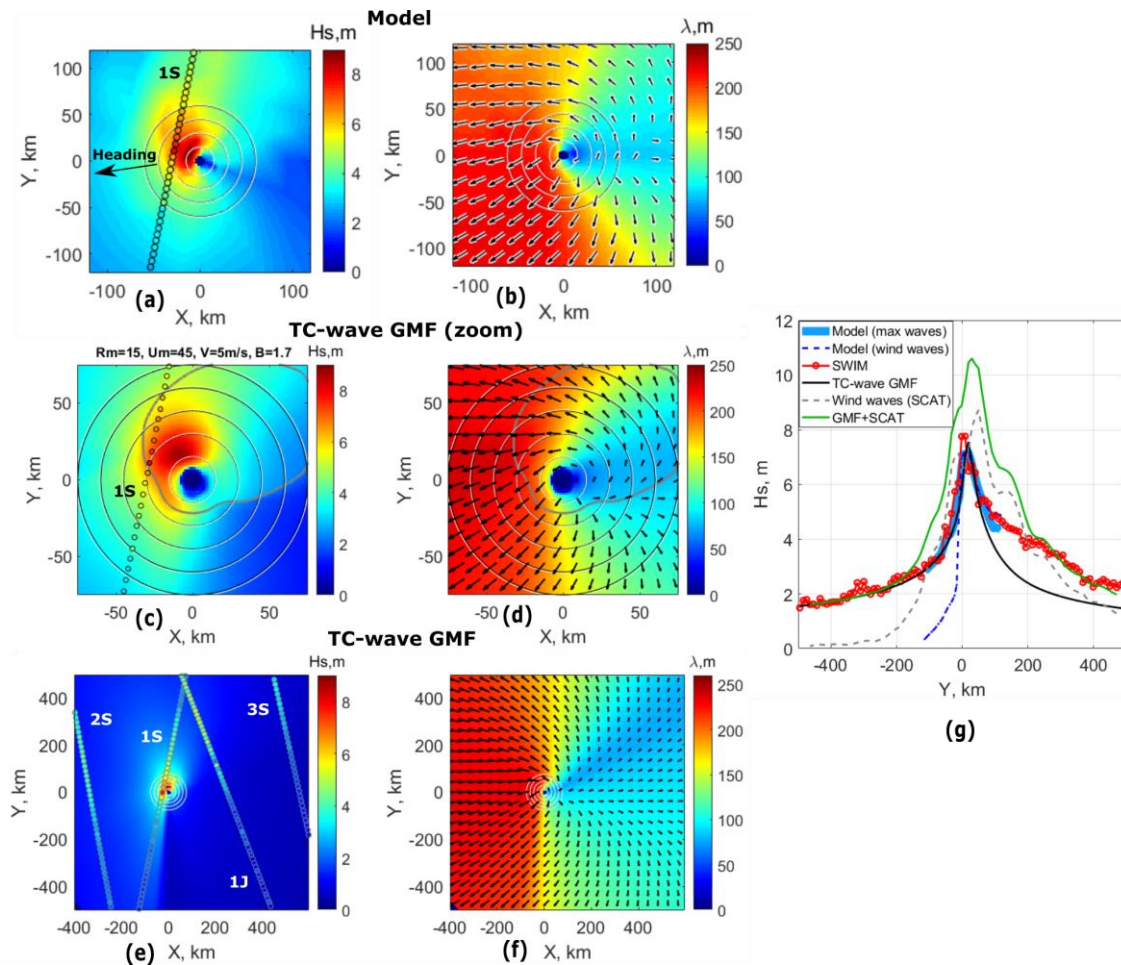
Figure 3. (a)-(b) Result of 2D parametric model calculation with wind input from SAR measurements: Hs and wavelength fields. (c)-(f) Hs and wavelength fields from TC-wave GMF. Colored circles are altimeter measurements. (g) Hs profiles along SWIM track 1S.

The other altimeter measurements (2S, 3S, 2J) were conducted far from TC center where the local wind is expected to be the dominant factor of wave energy formation. Superposition of wind waves (6) and swell (4) is presented on Fig. 4. Similar behavior and level of SCAT- and SWIM-derived Hs proves that wind waves in the far zone are indeed close to their full development and form the main input in total wave energy. Nevertheless, the account of swell is also important to obtain the correct Hs values.
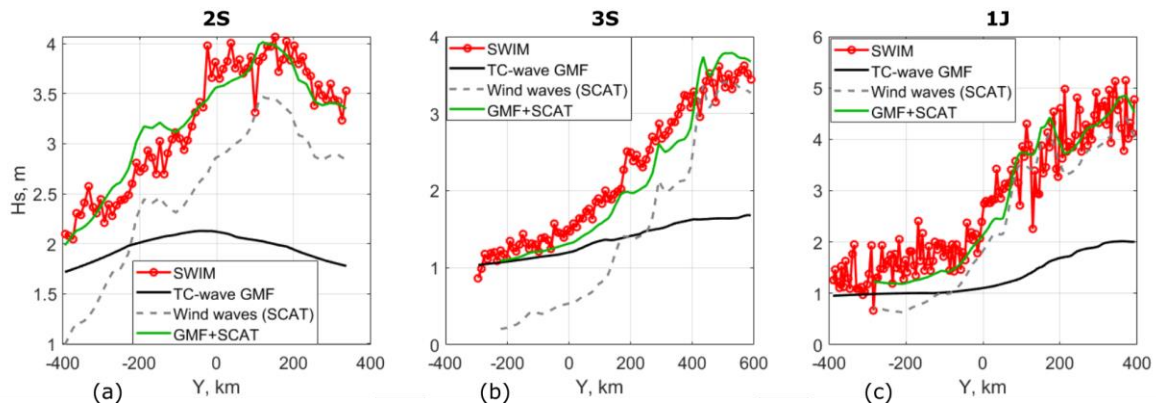

Figure 4. Hs profiles for tracks 2S (a), 3S (b) and 1J (c).

4.2. Wave Spectral Information

Besides Hs nadir measurements, SWIM instrument provides unique wave spectral information. Each discrete

acquisition of off-nadir rotating beam (colored circles on Fig. 5a) corresponds to transect of 2D angular spectrum in viewing direction. Thus, the whole rotation cycle (spiral branch on the sea surface) forms the full 2-dimensional spectrum averaged over the area ~100 km. Such resolution is too rough for TC with R_m ~10 km, but the spectral transects can be considered separately to compare the data with model at much higher resolution. For this, the analysis is performed for each SWIM beam acquisition inside the area 9 km x 9 km. The average wavelengths and wave directions of every modeled wave ray crossing this area are plotted in (λ_x, λ_y) coordinates (color dots on Fig. 5b)

together with respective characteristics of the peak of SWIM-derived 1D spectrum (black circle). Only the wave-train with maximum wavelength is further taken into account. If its direction is close to SWIM viewing azimuth (+-15º, accounting for 180º ambiguity), the respective wavelengths are compared. A scatter plot for all such points is presented in Fig. 5b. As obtained, the modeled and measured wavelengths generally agree, though the plot is quite scattered presumably due to the noise in SWIM data (see Fig. 5a). Notice, that though only three SWIM beams (6º, 8º, 10º) are usually used for spectral information (Liang et al., 2021), the correlation coefficients for measured and modeled wavelengths are similar for all beams (0.83, 0.76, 0.58, 0.8, 0.79 for incidence angles 2º, 4º, 6º, 8º, 10º, respectively).
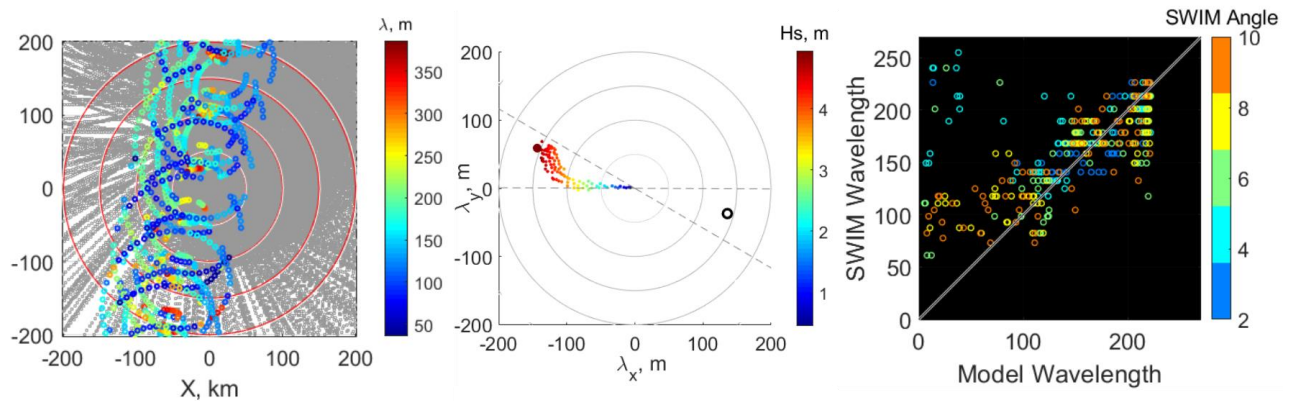

Figure 5. (Left) The modeled wave-rays (gray) and SWIM off-nadir measurements (2º, 4º, 6º, 8º, 10º incidence angles). Color indicates the peak wavelength of 1D spectrum. (Center) SWIM and model wavelength comparison. Color dots: average characteristics of model wave rays in the vicinity of one SWIM beam acquisition (black circle). The wave-train with maximum wavelength is taken into account only in a case if its direction lies between the two dashed lines indicating +-15º from SWIM observation azimuth. (Right) A scatter plot for all points satisfying the above criterion. Color is SWIM beam zenith angle.
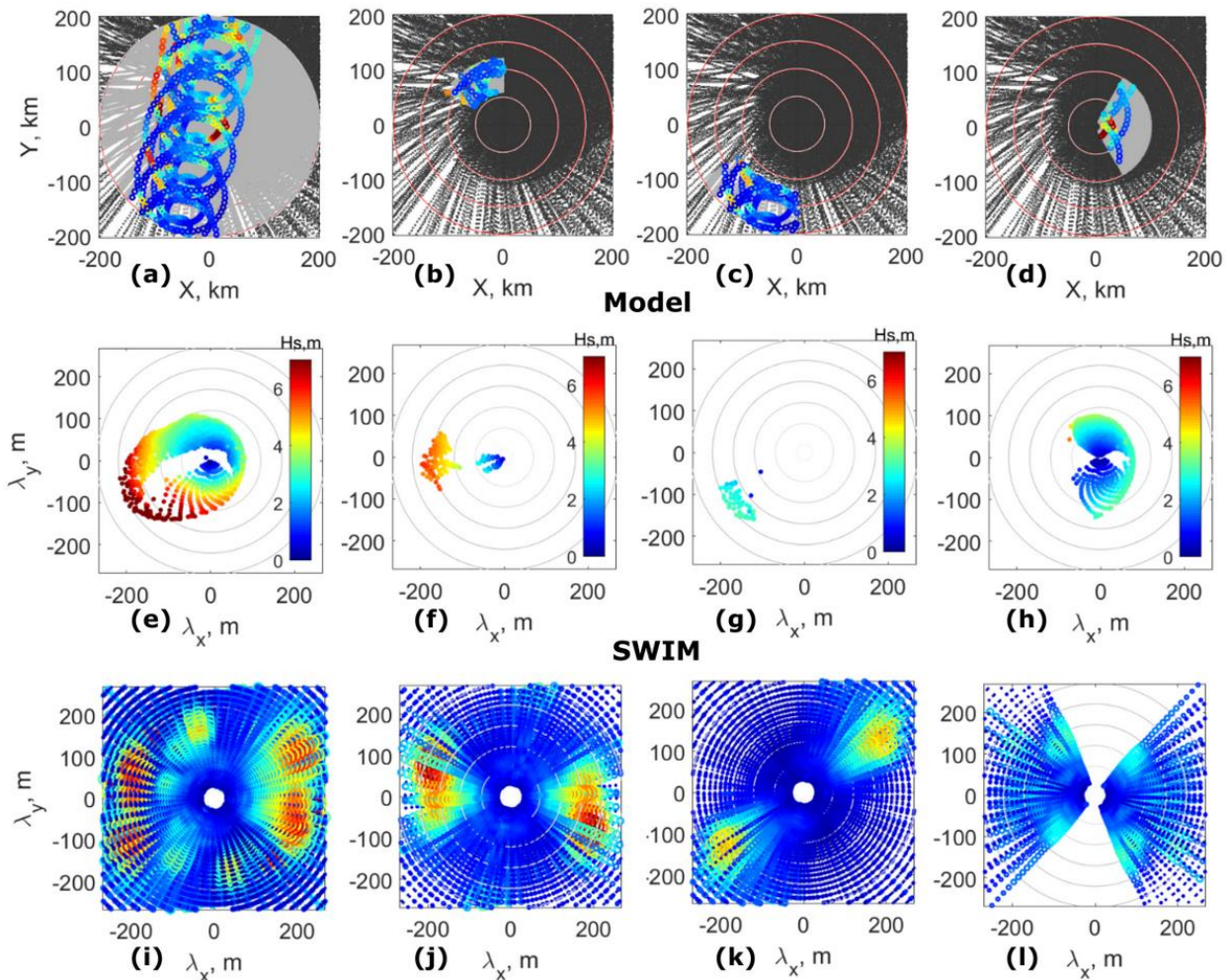
Figure 6. (a)-(c) The same as Fig. 4 (left) but for selected TC areas. (e)-(h) Characteristics of modeled wave-trains inside these areas (one point is one ray). (i)-(l) Superposition of SWIM 1D spectra for each beam in selected area.

Finally, the angular spectral characteristics are presented for different TC sectors, Fig. 6. The notations on subplots (a)-(h) are the same as on Fig. 5a-b, but for selected TC areas. The bottom subplots are SWIM 1D spectra organized accordingly to beam viewing direction. Though the comparison is quite indirect, both the model and SWIM reveal similar spectral features: wave intensification the right and forward TC sectors with wave directions shifted to the left, low-energy and multi-modal waving in the back sector and complicated spectral structure of the waves considered around TC eye in all azimuths at once. Wavelength and direction of spectral peaks agree quantitatively for model and observations.

5. CONCLUSION

A case study of TC Goni is presented as an example of joint analysis of CFOSAT SCAT/SWIM, Sentinel-1 SAR and altimeters data together with a recently developed 2D parametric model. The satellite measurements were obtained over the Philippine Sea on Oct. 29th, 2020, at the stage of TC intensification. The model for wave evolution inside TC is based on energy and momentum conservation laws. The equations are solved in the storm frame of reference using the wind field input from SAR estimates. The simplification of the model, i.e. generalized analytical self-similar solutions for wave development in TC conditions (TC-wave GMF), are considered as the first-guess estimate of significant wave height, wave length and direction fields. For GMF, the three TC parameters needed as input (maximum wind speed, TC radius and heading velocity) were taken from SAR-derived wind approximation by Holland (1980) function.

Estimates of both the direct model calculations and TC-wave GMF agree well with altimeter measurements in the vicinity of maximum winds and several TC radii apart. In the far zone, the local wind effects are found to dominate. CFOSAT SCAT wind data is then utilized to reproduce the correct Hs values, assuming that the wind waves are fully developed and follow Pierson-Moskovitz law.

The reconstructed two dimensional wave field structure inside TC Goni corresponds to general physical concepts and CFOSAT SWIM off-nadir measurements providing wave spectral information. Particularly, strong azimuth asymmetry is revealed, resulting from group velocity resonance between growing traveling waves and the moving TC in the front-right TC sector (the wave-trapping effect).

The study demonstrates the promising perspectives of combining the data from two CFOSAT instruments (SWIM and SCAT), satellite radars and altimeters and numerical modeling both for methods improvement (satellite data processing, model and TC-wave GMF refining) and for practical applications including prediction and prevention of hazards related with hurricane-generated extremely high waves.

REFERENCES

Donlon, C.; Berruti, B.; Buongiorno, A; Ferreira, M-H; Femenias, P. et al., 2012. The Global Monitoring for Environment and Security (GMES) Sentinel-3 Mission. Remote Sensing of the Environment. 120, pp. 27–57. doi:10.1016/j.rse.2011.07.024.

Duong Quoc-Phi, Langlade Sébastien, Payan Christophe, Husson Romain, Mouche Alexis, Malardel Sylvie, 2021. C-Band SAR Winds for Tropical Cyclone Monitoring and Forecast in the South-West Indian Ocean. Atmosphere, 12(5), pp. 576-603. doi.org/10.3390/atmos12050576

Hasselmann, K., Sell, W., Ross, D. B., Müller, P., 1976. A parametric wave prediction model. Journal of Physical Oceanography, 6, pp. 200–228.

Hauser D, Tourain C, Hermozo L, Alraddawi D, Aouf L, Chapron B, Dalphinet A, Delaye L, Dalila M, Dormy E, Gouillon F, Gressani V, Grouazel A, Guitton G, Husson R, Mironov A, Mouche A, Ollivier A, Oruba L, Piras F, Rodriguez Suquet R, Schippers P, Tison C, Tran N, 2021. New Observations From the SWIM Radar On-Board CFOSAT: Instrument Validation and Ocean Wave Measurement Assessment.

IEEE Transactions on Geoscience and Remote Sensing, 59(1), pp. 5–26. doi: 10.1109/TGRS.2020.2994372

Hauser D., Tourain C., Lachiver J.-M, 2019. CFOSAT : A new mission in orbit to observe simultaneously wind and waves at the ocean surface. Space Research Today, Elsevier, 206, pp.15-21. https://doi.org/10.1016/j.srt.2019.11.012

Holland, G. J., 1980. An analytic model of the wind and pressure profiles in hurricanes. Monthly Weather Review, 108, pp. 1212–1218. https://doi.org/10.1175/1520-0493(1980)108<1212:AAMOTW>2.0.CO;2

Kitaigorodskii, S. A., 1962. Applications of the theory of similarity to the analysis of wind-generated water waves as a stochastic process. Bulletin of the Academy of Sciences of the USSR Geophysics Series, 1, pp. 105–117.

Kudryavtsev, V., Golubkin, P., & Chapron, B., 2015. A simplified wave enhancement criterion for moving extreme events. Journal of Geophysical Research: Oceans, 120, pp. 7538–7558. https://doi.org/10.1002/2015JC011284

Kudryavtsev, V., Yurovskaya M. , Chapron, B., 2021. 2D parametric model for surface wave development in wind field varying in space and time. Journal of Geophysical Research: Oceans, 126.

Kudryavtsev, V., Yurovskaya, M., Chapron, B., 2021. Self-Similarity of Surface Wave Developments Under Tropical Cyclones. Journal of Geophysical Research: Oceans, 126.

Liang, G.; Yang, J.; Wang, J.,2021. Accuracy Evaluation of CFOSAT SWIM L2 Products Based on NDBC Buoy and Jason-3 Altimeter Data. Remote Sensing, 13, 887. https://doi.org/10.3390/rs13050887

Mouche Alexis, Chapron Bertrand, Zhang Biao, Husson Romain, 2017. Combined Co- and Cross-Polarized SAR Measurements Under Extreme Wind Conditions. IEEE Transactions On Geoscience And Remote Sensing, 55(12), pp. 6746-6755. https://doi.org/10.1109/TGRS.2017.2732508

Mouche Alexis, Chapron Bertrand, Knaff John, Zhao Yili, Zhang Biao, Combot Clement, 2019. Copolarized and Cross- Polarized SAR Measurements for High- Resolution Description of Major Hurricane Wind Structures: Application to Irma Category 5 Hurricane. Journal Of Geophysical Research: Oceans, 124(6), pp. 3905-3922. https://doi.org/10.1029/2019JC015056

Moon, I.-J., Ginis, I., Hara, T., Tolman, H. L., Wright, C. W., Walsh, E. J., 2003. Numerical simulation of sea surface directional wave spectra under hurricane wind forcing. Journal of Physical Oceanography, 33, pp.1680–1706, 2003. https://doi.org/10.1175/2410.1

Pierson, W. J., Jr, & Moskowitz, L., 1964. A proposed spectral form for fully developed wind seas based on the similarity theory of S. A. Kitaigorodskii. Journal of Geophysical Research, 69, pp. 5181–5190. https://doi.org/10.1029/jz069i024p05181

Young, I. R., 2017. A review of parametric descriptions of tropical cyclone wind-wave generation. Atmosphere, 8, 194. https://doi.org/10.3390/atmos8100194

Zhang, J. A., & Uhlhorn, E. W., 2012. Hurricane Sea Surface Inflow Angle and an Observation-Based Parametric Model. Monthly Weather Review, 140 (11), pp.3587-3605. https://doi.org/10.1175/MWR-D-11-00339.1